Estimation de la bande passante de détecteur infrarouges et impact sur la caractérisation thermique par Radiométrie Photothermique.

Estimation of infrared detector bandwidths and effect on the Pulsed Periodic Photothermal Radiometry performance.

Emmanuel RUFFIO[1*], Andrzej Kusiak[2], Clément Chassin[2], Jean-Luc Battaglia[2]

[1]AltRD, Co-actions Company, 46-48 rue Ferdinand Buisson, 33130 Begles (France)
[2]I2M-TREFLE, Univ. of Bordeaux, CNRS UMR 5295, cours de la Libération, 33400 Talence (France)
[*](Corresponding author: emmanuel.ruffio@alt-rd.com)

Résumé – La technique de radiométrie photothermique périodique en face avant (FF-PPTR) permet la caractérisation thermique d'échantillons à couches minces. Cette étude analyse les conditions expérimentales (bande passante du détecteur infrarouge et largeur de l'impulsion laser) requises pour la caractérisation d'un revêtement de $200\ nm$ d'épaisseur. Les temps de réponse de quatre détecteurs sont ensuite mesurés et comparés à l'aide d'un échantillon de référence. Le contenu fréquentiel de l'impulsion laser est également analysé.

Abstract – The Periodic Photothermal Radiometry setup in front face configuration (FF-PPTR) allows the investigation of multi-layered samples with low thicknesses. This work focuses on the experimental conditions (detector bandwidth and laser pulse width) required to estimate the thermal properties of a $200\ nm$ thick coating. Four infrared detectors are then compared based on their response time using a reference sample. A spectral analysis of the laser pulse is also performed.

Nomenclature

a	thermal diffusivity, $m^2.s^{-1}$
b	thermal effusivity, $W.K^{-1}.m^{-2}.s^{1/2}$
c_d	detector capacitance, F
C	capacitor impedance, Ω
f_c	cutoff-frequency, Hz
H	transfer function, $V.W^{-1}$
p	Laplace variable, s^{-1}
R	resistance, Ω
R	interfacial thermal resistance, $k.m^2.W^{-1}$
$t_{1/2}$	Half-rise time, s
Z	Impedance, Ω
Y	Output signal, V
T	temperature, K
Greek symbols	
β	unknown parameters
σ	standard deviation
τ	characteristic conduction time, s
Index and exponent	
c	relative to coating
f	relative to front face
k	relative to k^{th} filter
s	relative to substrate
laser	relative to laser

1. Introduction

The Periodic Pulse Photothermal Radiometry ([1], [2]) setup in front face configuration (FF-PPTR) allows the thermal characterization of multi-layered samples with layer thicknesses of a few hundred nanometers. The characteristic conduction time is such layers can be as low as of $10\ ns$ for low conductive material and may reach $1\ ns$. In such conditions, the esti-

https://doi.org/10.25855/SFT2025-093

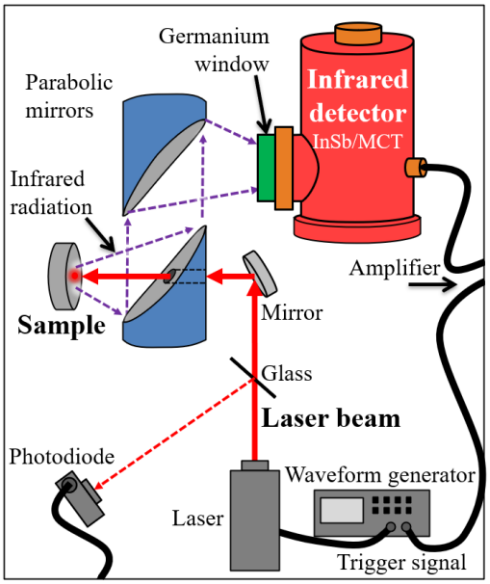

Figure 1: *Experimental setup of the Pulsed Periodic Photothermal Radiometry in front face configuration*

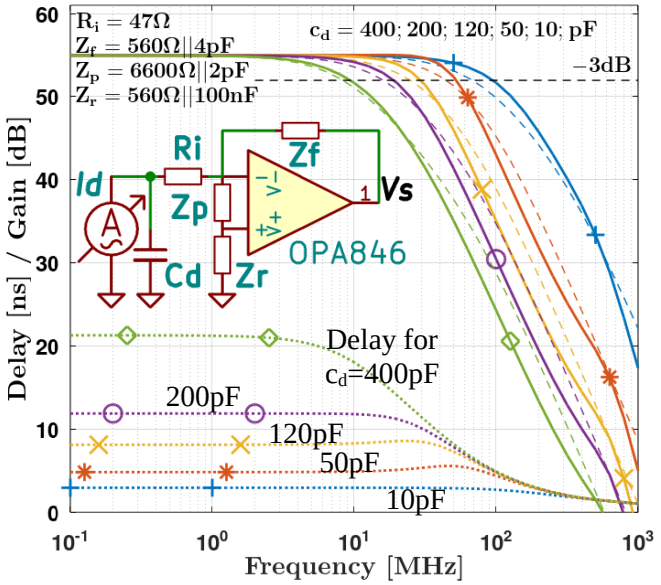

Figure 2: *Schematic of the first stage opamp of the detector amplifier and the corresponding gain and delay of the transfer function V_s/I_d versus detector capacitance c_d*

mation of the thermal properties, especially the diffusivity and the interfacial resistance, requires an experimental setup with the appropriate bandwidth to measure fast temperature variations. The bandwidth of the FF-PPTR method depends on the bandwidth of several components: (1) the laser pulse width whose frequency content is transferred to the sample, (2) the infrared (IR) detector, (3) the amplifier and (4) the acquisition system.

This work focuses on the laser and on the detector. An experiment design is first performed to identify the detector cut-off frequency and the laser pulse width required (or optimum) to estimate the thermal properties of a 200 nm thick coating. In section 2, the experimental setup and four N_2-cooled IR detectors are presented. A heat transfer model for the multilayer sample is derived using thermal quadrupoles (section 3). In section 4, the detector equivalent circuit and an electrical model of the new amplifier from AltRD Company are introduced. The emphasis is placed on the interaction between the first stage of the amplifier and the detector. The Maximum Likelihood Estimator is then applied to derive the expression of the standard deviation of the unknown thermal properties of the coating. In section 6, a sensitivity analysis of the temperature signal with respect to thermal properties is presented. The standard deviation of the coating diffusivity with respect to laser pulse width and detector cut-off frequency is shown and the optimal experimental conditions are identified. Finally, the IR detector response time are measured and compared (section 7). Finally, the real pulse waveform is measured and compared to the Gaussian approximation.

2. Description of the experiment

The setup is composed of a Coherent Matrix Q-switch Nd:YAG diode-pumped laser (1064 nm in wavelength) delivering continuously 10^4 pulses per second. One pulse is roughly similar to a Gaussian curve with standard deviation $\sigma_{laser} = 10$ to 14 ns depending on laser power setting. A small part (< 2%) of the beam is reflected back to a photodiode (THORLABS DET10, 350 MHz@632 nm) by a 1mm thick glass (microscope slide glass) to monitor the pulse waveform. The laser beam is redirected by a mirror and the beam radius at the sample surface is about 1.75 mm. The infrared radiation emitted by the sample is collected by two

parabolic mirrors with focal length $50.8\,mm$ towards a photovoltaic infrared detector. Four infrared detectors are considered and compared in this work:

(1) Judson J10D-M204-R100U (InSb, active area 0.01mm², 10pF, 1-5µm),
(2) Infrared Associates 2C-1.0 (InSb, active area 0.79mm², 120pF, 2.5-5.5µm)
(3) Kolmar Tech. KMPV11-1-J1/Ge with preamp. (MCT, active area 1mm², 5.5-13µm)
(4) Infrared Associates MCT-13-0.5PV (MCT, active area 0.20mm², 5.5-13µm)

The three detectors (1), (2) and (4) are connected to a high-speed amplifier (RD-HS2PV) with a gain equal to $1.4 \times 10^6 V/A$ and a cut-off frequency of $f_c = 40Mhz@-3dB$. The Kolmar (3) detector has its own integrated amplifier with $f_c = 20\,MHz$. A 2mm thick germanium (Ge) window with spectral range $6\text{-}12\mu m$ is placed on each detector to filter the diffuse reflections of the laser. The signals from both the photodiode and the IR detector amplifier are recorded using a Picoscope 9000 ($12GHz$, 16 bits) or an oscilloscope Lecroy WaveRunner LT364 ($500MHz$, 8 bits ADC, 16 bits for math operations) depending on the signal voltage amplitude. The laser pulse and the acquisition are triggered by a waveform generator (Agilent 33220A). With the PPTR method, the temperature signal is not measured after one laser pulse, but is instead averaged over hundreds or thousands of pulses which significantly reduces the noise.

3. Thermal modeling of the sample

Let consider a sample constituted of two layers, denoted the coating and the substrate with an interfacial thermal resistance R. Thermal properties are assumed isotropic and uniform and are respectively $\lambda_c, \rho C_c$ and $\lambda_s, \rho C_s$. Since the sample and the detector sensitive element are at the focal point of the parabolic mirrors, only the temperature at the center of the laser beam is recorded. As a result, the heat transfers are mainly one-dimensional for short times. Neglecting convective and radiative heat losses and assuming the coating is opaque, the front face temperature T_f(t), or T_f(p) in Laplace domain, is given using thermal quadrupoles [3]:

$$\begin{bmatrix} T_b(p) \\ 0 \end{bmatrix} = \begin{bmatrix} A_s & B_s \\ C_s & D_s \end{bmatrix} \begin{bmatrix} 1 & R \\ 0 & 1 \end{bmatrix} \begin{bmatrix} A_c & B_c \\ C_c & D_c \end{bmatrix} \begin{bmatrix} T_f(p) \\ \phi(p) \end{bmatrix}$$

$$with \begin{bmatrix} A_x & B_x \\ C_x & D_x \end{bmatrix} = \begin{bmatrix} \cosh\left(\sqrt{p\tau_x}\right) & \dfrac{1}{b_x\sqrt{p}} \sinh\left(\sqrt{p\tau_x}\right) \\ b_x\sqrt{p}.\sinh\left(\sqrt{p\tau_x}\right) & \cosh\left(\sqrt{p\tau_x}\right) \end{bmatrix} \quad (1)$$

With $\phi(p) = L(\phi(t))$ the Laplace transform of the laser power absorbed by the sample. With $T_b(p)$ the back face temperature. With $b_x = \sqrt{\lambda_x \rho C_x}$ the thermal effusivity, $\tau_x = e_x^2/a_x$ the characteristic conduction time with e_x and a_x the layer thickness and thermal diffusivity respectively, for layer $x = \{coating, substrate\}$. Let $th(x)$ the tangent hyperbolic function and H_{th}(p) the transfer function related to conduction heat transfer, Eq.(1) becomes:

$$H_{th}(p) = \frac{T_f(p)}{\phi(p)} = \frac{\eta}{R_c} . \frac{1 + \frac{b_s}{b_c} th\left(\frac{\tau_s}{\tau_c}\eta\right)\left[\frac{R}{R_c}\eta + th(\eta)\right]}{\frac{b_s}{b_c} th\left(\frac{\tau_s}{\tau_c}\eta\right)\left[1 + \frac{R}{R_c}\eta . th(\eta)\right] + th(\eta)} \text{ with } \eta = \sqrt{p\tau_c} \quad (2)$$

With $R_c = e_c/\lambda_c$ the thermal resistance of the coating. If the characteristic conduction time of the coating is large compared to the acquisition time window, the model reduces to the semi-infinite case:

$$H_{th}(p) = \frac{T_f(p)}{\phi(p)} = \frac{1}{b_c\sqrt{p}} \quad (3)$$

4. Mathematical modeling of the IR detectors and the amplifier

The amplifier used in this work was designed to operate with the three detectors mentioned above. The first stage of the amplifier (Figure 2) is the most critical. It is based on the voltage feedback operational amplifier OPA846 [4]. To avoid confusion with the term "amplifier", operational amplifiers are denoted "opamp" in this document. The IR detector is replaced by its equivalent circuit [5] (an ideal current source in parallel with the detector junction capacitance c_d). The junction shunt resistance and junction diode are neglected.

Despite following the guidelines of the datasheet [4], this opamp was only stable with J10D detector and could not be stabilized for the two others whose capacitance is significantly higher (120pF >> 10pF). An additional series resistance R_i was therefore introduced to isolate the opamp from the detector capacitance. It leads to a slight drop of performance but this approach was chosen nonetheless to keep the same amplifier for all detectors. Let $H_1(p)$ be the transfer function of the 1st-stage opamp. Using Kirchhoffs current Law, the output voltage $V_s(p)$ with respect to detector current $I_d(p)$ induced by incoming infrared radiation, is:

$$H_1(p) = \frac{V_s(p)}{I_d(p)} = \frac{-Z_f}{1+\frac{R_i}{C_d}} \frac{1}{1+\frac{1}{Z}\left[1+\frac{Z_f}{Z_p}\left(1+\frac{Z_r}{Z_f}+\frac{Z_p+Z_r}{C_d+R_i}\right)\right]} \qquad (4)$$

With $C_d(p), Z_f(p), Z_s(p), Z_r(p)$ the impedances shown in Figure 2 and $Z(p)$ the open loop gain of the opamp with $V_s(p) = Z(p)\big(V^+(p) - V^-(p)\big)$. The common-mode impedance, the offset voltages, the input capacitance and the output impedance are neglected. The transimpedance gain of the first stage is set by Z_f and is $560\ V/A$. Using [4], $Z(p)$ is approximated between 0 and 1 GHz by combining a 1st-order low-pass filter and a time delay:

$$Z(p) = \frac{A}{1+\frac{p}{2\pi f_a}} \frac{1-\frac{p}{2\pi f_b}}{1+\frac{p}{2\pi f_b}} \quad \text{with} \quad \begin{cases} A = 90\ dB \\ f_a = 23\ kHz \\ f_b = 500\ MHz \end{cases} \qquad (5)$$

Figure 2 presents the frequency response of $H_1(p)$ with respect to the detector capacitance c_d from 10 to $400pF$. Dashed lines refer to the first-order low-pass filter approximation (first part of Eq.(4)) with cutoff frequency $f_1 \approx 1/(2\pi R_i c_d)$. Dotted lines refer to the delay (in ns) induced by $H_1(p)$. The capacitance of detector (1) J10D being only $10pF$, this figure shows that the delay induced by this first opamp is constant up to $100MHz$. If the temperature signal bandwidth is lower than $100MHz$, the only effect of $H_1(p)$ is to delayed (shift) the signal.

The output signal then goes through other amplifier stages before the acquisition device. The transfer function $H(p)$ of these stages can be modelled by chaining 6 first-order low-pass filters, denoted $H_2(p) \dots H_7(p)$. These filters are mostly parasitic filters due to opamp limitations. Let $(f)_k$ with $1 \le k \le 7$ denotes the cut-off frequency vector of the entire analogue signal chain with f_1 being the cut-off frequency of $H_1(p)$. It comes $f = [f_1; 80;\ 80; 130;\ 300; 300; 600]\ MHz$. An additional first-order low-pass filter with $f_c = 500\ MHz$ must be added if the Lecroy scope is used. The output signal $Y(p)$ is then:

$$Y(p) = H_7(p) \dots H_1(p)\ G_{optic}\ H_{th}(p)\ \phi(p) \quad \text{with}\ H_{k\ge 2}(p) = \frac{1}{1+p/(2\pi f_k)} \qquad (6)$$

With G_{optic} the gain of the optical path including, the shape factor, the IR emission of the sample, the detector efficiency, the parabolic mirrors, the Ge and detector windows.

5. Experiment design

To assess whether it is possible to estimate the thermal properties of the coatings and the interfacial resistance, an experiment design analysis is carried out. It consists in computing the theoretical standard deviations of unknown parameters β considering they are estimated with the Maximum Likelihood estimator (MLE). Assuming the measurement noise is independent, identically distributed and Gaussian with standard deviation σ_m, the MLE reduces to least squares and the objective function is:

$$J(\beta) = \big(Y^*(t) - Y(t)\big)^T \big(Y^*(t) - Y(t)\big) \qquad (7)$$

With Y^* a column vector containing the N_s measurements and $Y(t)$ the model outputs. The estimations $\hat{\beta}$ are found by minimizing $J(\beta)$ and the normalized standard deviations $std^*(\hat{\beta})$ are given by the diagonal coefficients of the covariance matrix [6]:

$$std^*(\hat{\beta}) = \frac{std(\hat{\beta})}{\hat{\beta}} = \left[\frac{\sigma_{\beta 1}}{\beta_1}, \dots, \frac{\sigma_{\beta N}}{\beta_N}\right]^T = \sqrt{\mathrm{diag}(\sigma_m^2 [X^T X]^{-1})} \text{ with } X = \hat{\beta}\frac{\partial Y}{\partial \beta}(\hat{\beta}) \qquad (8)$$

With $X(\hat{\beta})$ the reduced sensitivity matrix of the model outputs. Since σ_m is only a scaling value, it is set to $1/\sqrt{N_s}$ so that $std^*(\hat{\beta})$ is nearly independent of the acquisition frequency.

6. Results: Effect of cut-off frequency and laser pulse width

Let consider we want to use the amplifier described in section 4 to estimate the thermal properties of a $200nm$ thick silicon nitride (SiN) coating over a $750\ \mu m$ thick silicon substrate [2] whose properties are known. There are then 5 unknown parameters $\beta = \left[G_{optic}; b_c; a_c;\ R; f_1\right]^T$: the optical gain, coating effusivity and diffusivity, the interfacial resistance and the first cut-off frequency (detector + first opamp). Using the De Hoog algorithm for the inverse Laplace transform with Eq.(6), Figure 3 shows the temperature response $Y(t)$ of the sample for a coating thickness $e_c = 200$ and $500\ nm$. The semi-infinite case ($e_c = \infty$) is also presented for comparison. It shows that a $500\ nm$ thick coating is close to behave like a semi-infinite sample ($\tau_c = 400\ ns$). It also shows that the acquisition time window must be large enough to estimate a_c and R since it requires the heat wave to bounce at the interface and to come back at the surface. For $e_c = 200\ nm$ and $e_c = \infty$, the effect of the detector cut-off frequency f_1 is presented: dashed and dotted lines refer to $f_1 = 50\ MHz$ and $10\ MHz$ respectively. To estimate the delay induced by the analog chain, the half-rise time $t_{1/2}$ is also presented (thin black circles). With no filtering, the delay is $t_{1/2} = 7.4\ ns$ and is increased by $\Delta t_{1/2} = 16.4 - 7.4 = 9\ ns$ for $f_1 = 50\ MHz$. This value can be compared to the theoretical delay $\delta(f)$ of the analog chain computed by summing the delay of each filter. Assuming signal frequencies are lower than all f_k, i.e., $f \ll f_{1 \le k \le 7}$, $\delta(f)$ is constant equal to 9.7 ns:

$$\delta(f) = -\frac{1}{2\pi f}\mathrm{angle}\big(H(f)\big) = \sum_{k=1}^{7} \frac{\mathrm{atan}(f/f_k)}{2\pi f} \approx \sum_{k=1}^{7} \frac{1}{2\pi f_k} = 9.7\ ns \qquad (9)$$

For $f_1 = 10\ MHz$, $t_{1/2}$ is increased by $\Delta t_{1/2} = 15.5\ ns$ whereas $\delta = 22\ ns$. The discrepancy becomes significant since the assumption $f \ll f_{1 \le k \le 7}$ does not hold anymore.

The reduced sensitivities $X(t)$ (Figure 4) show two pairwise correlations: (1) between G_{optic} and b_c and (2) between R and a_c. Moreover, the sensitivity to R is much lower than the others. To analyse more precisely the correlations between the 5 unknown parameters, a SVD decomposition of matrix $X = U.S.V^T$ is used to retrieve the singular values $(S)_{i,i} = [29; 6.0; 2.1; 0.71; 0.005]$ of X. It clearly results in a bad condition number $\mathrm{cond}(X^T X) = 4.0 \times 10^7$ and the inverse problem is ill-posed. By looking into the matrix V, the smallest

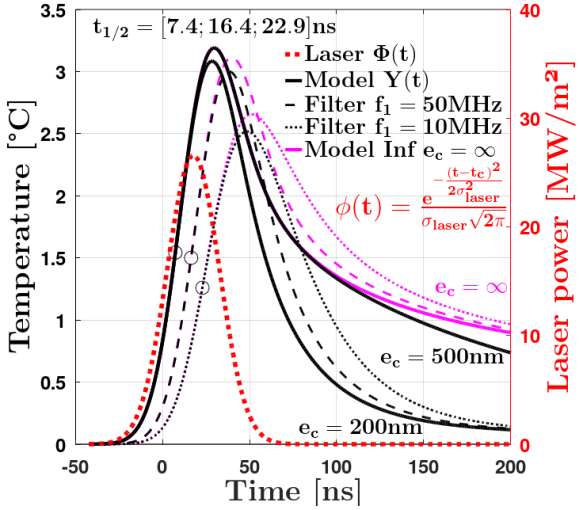

Figure 3: *Temperature response of the sample to a laser pulse versus coating thickness e_c and detector cutoff frequency f_1.*

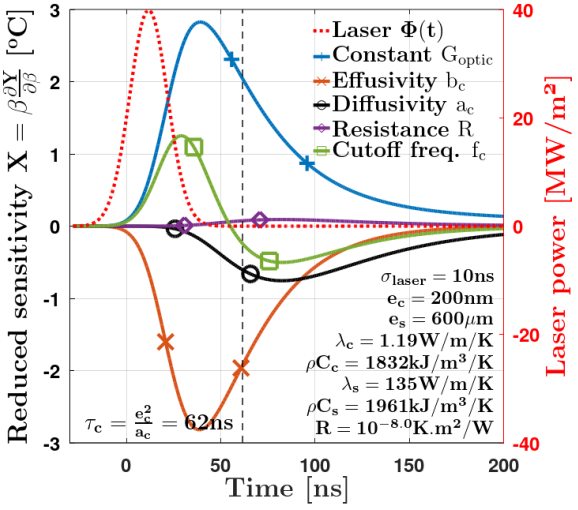

Figure 4: *Reduced sensitivity with respect to unknown parameters and reference values used for the computation.*

singular value is associated with the correlation of a_c and R. It means that the effect on $Y(t)$ due to a change of a_c can be compensated in a large extent by R. Estimating these parameters simultaneously will be difficult. If f_1 is decreased to $10\ MHz$, the situation gets worse with $\text{cond}(X^TX) = 21 \times 10^7$ and with $f_1 = 100\ MHz$, the improvement is small with $\text{cond}(X^TX) = 3.3 \times 10^7$. The same conclusion holds if f_1 is assumed known.

To visualize how the experiment configuration alters the quality of estimations, contour map of $std^*(a_c)$ (see Eq.(8)) is shown in Figure 5. Computations are based on properties given in Figure 4 and for this first example, f_c is assumed known, i.e., the 4 unknowns are $\beta = [G_{optic}; b_c; a_c; R]$. Only the results for the coating diffusivity are presented since its estimation is difficult. The contour maps of the other parameters are generally quite similar. As expected, $std^*(a_c)$ is decreased with shorter pulse width and high cut-off frequency. Let define the optimum area with a contour value lower than 1. It is quite large in this case ($\sigma_{laser} < 20\ ns$ and $f_1 > 7MHz$) and not so difficult to get in practice. If the detector cut-off frequency f_1 is now considered unknown (Figure 6) and has to be estimated, the optimum area is shifted towards shorter pulse and higher cut-off frequency ($\sigma_{laser} < 10\ ns$ and $f_1 > 20MHz$). If σ_{laser} is increased beyond $50\ ns$, $std^*(a_c)$ increases rapidly.

In previous figures, the energy of one pulse is assumed constant regardless of the pulse width which implies an increase of the power. In Figure 7, two changes are made: (1) the

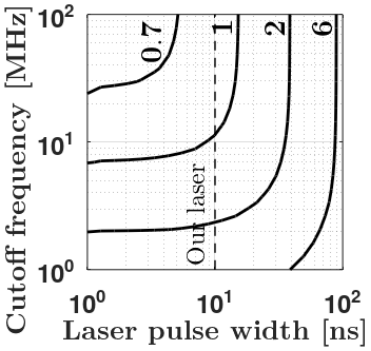

Figure 5: *Normalized standard deviation of diffusivity a_c versus f_1 and σ_{laser}.*

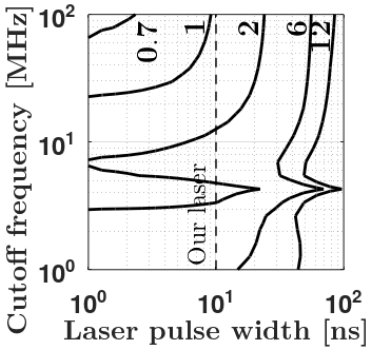

Figure 6: *Normalized standard deviation of diffusivity a_c with f_1 considered unknown.*

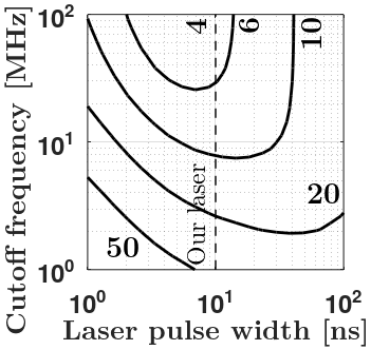

Figure 7: *Normalized standard deviation of a_c with constant power and $e_c = 50\ nm$.*

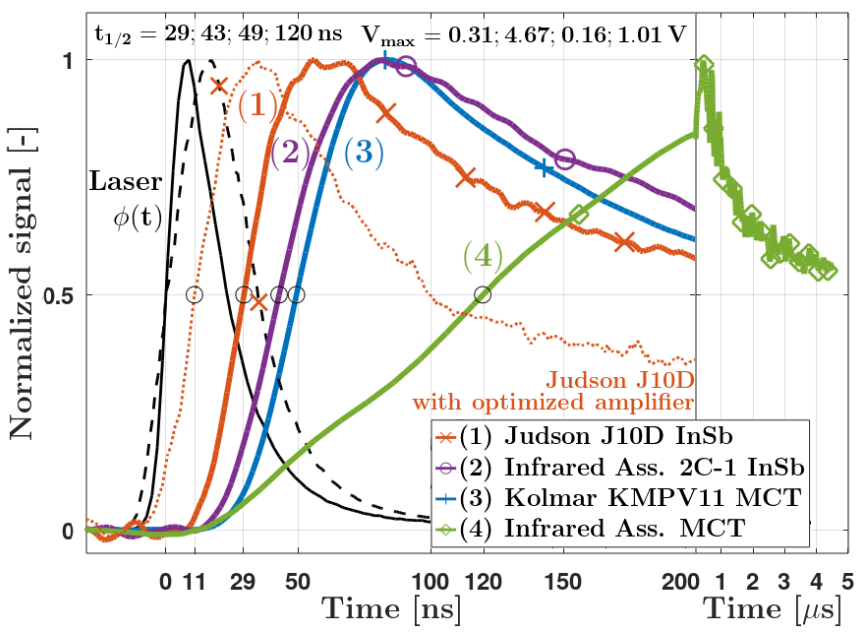

Figure 8: *Temperature signal for each infrared detector (1) to (4) following the laser pulse $\phi(t)$ and signal with an optimized amplifier for the detector Judson J10D (1) (dotted line)*

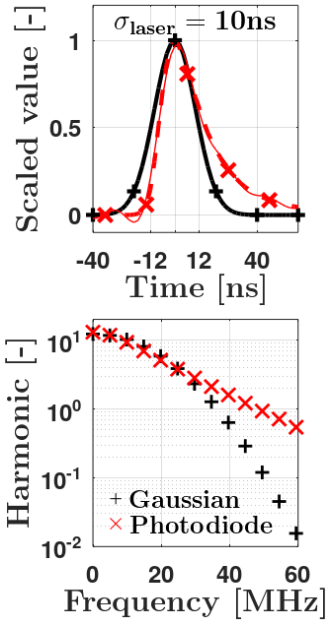

Figure 9: *Gaussian laser waveform vs photodiode signal: signal (top) and spectrum (bottom)*

pulse power is now constant so that the amount of energy is proportional to σ_{laser} and (2) the coating is thinner ($e_c = 50\,nm$). There is now an optimum value for the pulse width around $\sigma_{laser} = 6\,ns$ and $f_1 = 100MHz$. The corresponding laser full-width at half maximum is $\Delta_{laser} = 2\sqrt{2\ln(2)}.\sigma_{laser} = 14\,ns$. Based on these analyses, the laser used in this work ends up being very appropriate since its pulse width is close to the optimum.

7. Results: comparison of infrared detector response times

The four N_2-cooled detectors mentioned previously are now compared by measuring the half-rise time of a temperature signal induced by a laser pulse on an aluminium sample covered with a black paint. The thickness of the black paint is likely to be higher than $10\,\mu m$ which leads to a characteristic conduction time greater than $800\,\mu s$. The sample is then assumed semi-infinite. As shown by Eq.(3), the shape of the normalized signal is independent of the thermal properties since the effusivity is only a scaling factor. The signals measured by each detector with the corresponding half-rise times are presented in Figure 8. The J10D (1) is the fastest with $t_{1/2} = 29ns$, followed by the Infrared Ass. (2) and the Kolmar (3) ($t_{1/2} = 43$ and $49ns$ respectively). The Infrared Ass. (4) is much slower and exhibits a strange linear signal for $t \in [10; 200]\,ns$. It looks like a capacitor is being charged by a constant current. The black dashed line refers to the pulse waveform measured when using the detector J10D (1). This different pulse waveform is probably due to a misconfiguration of the laser since for the three other cases, they perfectly match.

The benefit of a very small active area, 0.01mm² for the J10D (1), is to increase the speed by decreasing the capacitance. The drawback is to reduce the sensitivity. The signal amplitude is indeed 15 times lower than the Infrared Ass. (2), respectively $V_{max} = 0.3\,V$ and $4.7\,V$. It could be worse since the active area is 80 times smaller. With the Kolmar (3), the signal amplitude is only $0.2V$ which seems small regarding the high sensitivity of its MCT element. This is due to its integrated amplifier whose gain differs from the RD-HS2PV amplifier. It should be noticed that the noise level of the Kolmar (3) is remarkably low.

The dotted line (Figure 8) refers to an experiment where the Judson J10D (1) was used with an optimized version of the RD-HS2PV amplifier. By targeting only one detector, the amplifier topology and its components could be adjusted to increase the bandwidth. The multilayer sample used here differs from the one used previously which probably explains the slope change at $t = 100\,ns$. With this dedicated amplifier, $t_{1/2}$ could be reduced from 29 ns to $11\,ns$. Subtracting the delay of $7.4\,ns$ due to heat conduction (Figure 3), the delay induced by the amplifier is about $\delta = 4\,ns$. Considering there are 7 first-order low-pass filters in the amplifier, the average cut-off frequency of each filter is $280\,MHz$. The uncertainty of this value may be large since the coaxial cable lengths and the photodiode delay are neglected.

In Figure 9, the Gaussian shape (black) used for the experiment design is compared to the pulse waveform measured by the photodiode. The harmonics up to $60\,MHz$ are also presented which reveals a surprising linear trend for the photodiode signal. The thin red line is the pulse shape with its spectrum clamped at $40\,MHz$. It shows most of the pulse waveform is contained below this frequency. As the front face temperature depends linearly on the pulse harmonics, the temperature signal contains only these harmonics, out of phase and attenuated.

8. Conclusion

Based on the sensitivity analysis, the most difficult parameters to estimate are the coating thermal diffusivity and the interfacial thermal resistance. The experiment design showed that the estimation uncertainty of the thermal diffusivity of a $200\,nm$ thick coating is reduced by decreasing the laser pulse width and increasing the detector bandwidth. When the pulse energy is assumed constant regardless of the pulse width, there is no optimum. However, if the laser power is now fixed, the optimum configuration for a $50\,nm$ thick coating involves a 100 MHz bandwidth detector and a laser pulse full-width of $14\,ns$ ($\sigma_{laser} = 6\,ns$). Considering our laser ($\sigma_{laser} = 10\,ns$) and using a $350\,MHz$ photodiode, a spectrum analysis of the pulse waveform revealed that most information is contained below $40\,MHz$. The objective for the analogue signal chain is to keep the information attenuation and distortion as low as possible.

The response times of four N_2-cooled IR detectors were then measured. Thanks to its very low capacitance, the Judson J10D detector won the race by a good margin with a half-rise time of $29\,ns$, at the expense of sensitivity. As the response-time is related to the amplifier topology, it was shown the limiting factor is not the J10D detector. The half-rise time could be indeed further reduced to $11\,ns$ by using an amplifier designed by AltRD and optimized for that detector. Further developments will be attempted to reach the detector limit.

References

[1] J.-L. Battaglia, E. Ruffio, A. Kusiak, C. Pradere, E. Abisset, S. Chevalier, A. Sommier, J.-L. Batsale, The periodic pulse photothermal radiometry technique within the front face configuration, *Measurement*, 158 (2020).

[2] C. Chassin., A. Kusiak, K. Krause, M. Garcia, J-L. Battaglia, Bayesian Estimation of Thermal Properties Using Periodically Pulsed Photothermal Radiometry: A Focus on Interfacial Thermal Resistances between Layers, *Phys. Status Solidi RRL*, 17 (2023).

[3] D Maillet, S Andre. J. Batsale, A. Degiovanni, and C. Moyne, *Thermal Quadrupoles* (2000).

[4] Texas Instrument, OPA846, Wideband, Low-Noise, Voltage-Feedback Operational Amplifier, SBOS250E, December (2008).

[5] Teledyne, Judson Technologies, Indium Antimonide Detector (2003).

[6] D. Petit, D. Maillet, Techniques inverses et estimation de paramètres. Partie 2, *Techniques de l'Ingénieur*, AF4516 v1 (2019)